The Effect of Conducting Boundaries on Weakly Nonlinear Darcy–Bénard Convection

D. Andrew S. Rees · Abdelkader Mojtabi

Abstract We consider convection in a uniform fluid-saturated porous layer which is bounded by conducting plates and heated from below. The primary aim is to determine the identity of the postcritical convection planform as a function of the thicknesses and conductivities of the bounding plates relative to that of the porous layer. This work complements and extends an early paper by Riahi (J Fluid Mech 129:153–171, 1983) who considered a situation where the porous layer is bounded by infinitely thick conducting media. We present regions in parameter space wherein convection in the form of rolls is unstable and within which cells with square planform form the preferred pattern.

Keywords Porous media · Convection · Weakly nonlinear analysis · Dispersion relation · Square cells · Convective rolls

List of Symbols

$\mathcal{A}$	Arbitrary constant
A, B, C	Roll amplitudes
c_1, c_2, c_3	Constants in amplitude equations
c.c.	Complex conjugate
C	Heat capacity
d	Conductivity ratio
f, g	Functions in weakly nonlinear theory
$\mathcal{F}$	Dispersion relation
$\bar{g}$	Gravity

D. A. S. Rees (✉)
Mechanical Engineering, University of Bath, Bath, BA2 7AY, UK
e-mail: ensdasr@bath.ac.uk

A. Mojtabi
INPT, UPS; IMFT (Institut de Mécanique des Fluides de Toulouse), Université de Toulouse, Allé Camille Soula, 31400 Toulouse, France

h	Height of sublayer
k	Disturbance wavenumber
K	Permeability
p	Pressure
Ra	Darcy–Rayleigh number
t	Time
T	Dimensional temperature
u, v	Horizontal velocities
w	Vertical velocity
x, y	Horizontal coordinates
z	Vertical coordinate

Greek Symbols

α	Disturbance wavenumber
β	Expansion coefficient
γ	Equal to d/δ
δ	Sublayer thickness ratio
ΔT	Reference temperature drop
ϵ	Small quantity
θ	Temperature
Θ	Disturbance temperature
κ	Thermal diffusivity ratio
λ	Function of Ra and α
μ	Dynamic viscosity
ρ	Density
σ	Function of Ra and α
τ	Slow time scale
ϕ	Relative orientation of two rolls
Ω	Coupling coefficient

Subscripts and Superscripts

c	Critical conditions
f	Fluid
m	Iteration number
ref	Reference value
1, 2, 3, ...	Context-dependent meanings
$\hat{}$	Dimensional quantity
$\bar{}$	Reduced disturbance
$'$	Derivative with respect to z

1 Introduction

Convection in a horizontal porous layer heated from below has attracted a large amount of attention due, in part, to its widespread applications in engineering and industrial processes. In its most basic form, namely, a horizontal layer of uniform thickness subject to Darcy's

law, the Boussinesq approximation and a constant temperature drop, it forms one of the simplest linear instability problems involving a coupled pair of partial differential equations, and therefore may be used to great effect for teaching purposes. The first papers which studied the onset problem are those by Horton and Rogers (1945) and Lapwood (1948), and this generic stability problem is named either as the Horton–Rogers–Lapwood problem or as the Darcy–Bénard problem. While a weakly nonlinear analysis for the classical Darcy–Bénard problem also proceeds analytically [see Rees and Riley (1989a,b) and Rees (2001)], it becomes necessary to resort to numerical methods for any system which is more complicated; see Riahi (1983) and Rees and Riley (1990). State-of-the-art reviews of these matters and related convection problems may be found in the chapters by Rees (2000), Tyvand (2002), Rees et al. (2008) and Nguyen-Quang et al. (2010), and the books by Pop and Ingham (2001) and Nield and Bejan (2006).

Layered porous media are ubiquitous in both nature and industrial applications, and numerous studies have been made of these cases. Although it was not the first paper on the topic, a very comprehensive analysis of the onset of convection was undertaken by McKibbin and O'Sullivan (1980), who considered two- and three-sublayer configurations. It was found that the neutral curve sometimes exhibits two local minima thereby allowing the identity of the critical mode of convection to change discontinuously as the system parameters change smoothly. Further work on the onset of convection in layered media may be found in McKibbin and Tyvand (1983) and Postelnicu (1999). This work was later extended into the weakly nonlinear regime by McKibbin and O'Sullivan (1981). Rees and Riley (1990) also provided a weakly nonlinear stability analysis and showed that some configurations give rise naturally to three-dimensional convection patterns. A similar conclusion was obtained earlier by Riahi (1983), who considered a classical Darcy–Bénard layer sandwiched between two conducting solid regions. Other works on layered media have been undertaken by Masuoka et al. (1979) and Rana et al. (1979) and, more recently, on layers where fluid movement is confined to each sublayer by impermeable but infinitesimally thin partitions, by Genç and Rees (2011) and Rees and Genç (2011).

The aim of the present work is to determine how the presence of conducting boundaries affects the identity of the pattern of convection which arises immediately post onset. To this end a weakly nonlinear analysis is performed. Although this mathematical problem is governed by four nondimensional parameters, namely two conductivity ratios and two thicknesses for the conducting layers, it is possible to gain a fairly complete understanding of the circumstances in which rolls are preferred, and those in which square cells are preferred.

2 Problem Formulation and Basic State

The aim of this study is an investigation of the effect of conducting boundaries on the onset of convection and the subsequent weakly nonlinear pattern selection. The main objective is to delineate the regions in parameter space within which one might expect square cell convection (as viewed from above) or rolls. The detailed configuration we consider is shown in Fig. 1 and it comprises a uniform isotropic saturated porous layer of thickness, h_2, which is bounded by two uniform, impermeable but thermally conducting plates of thicknesses, h_1 and h_3. These plates do not necessarily have identical conductivities or thicknesses. Moreover the conductivities are generally different from that of the porous layer. This composite layer is of infinite extent in both horizontal directions. The present paper may be regarded as an extension of the work by Riahi (1983) in which both h_1 and h_3 were taken to be infinite.

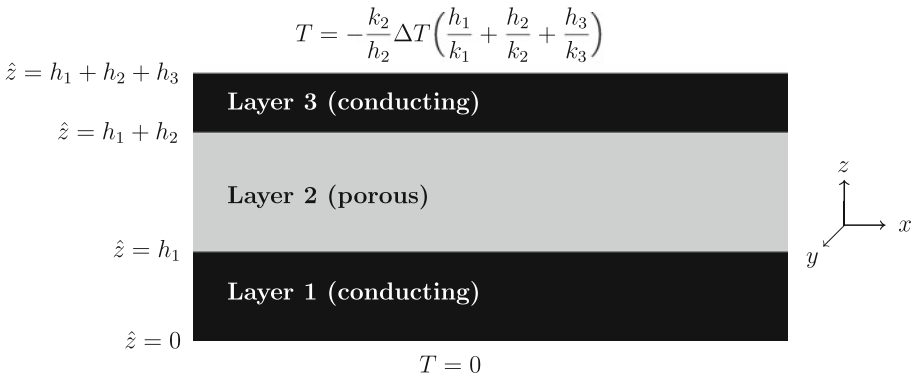

Fig. 1 Geometry of the porous layer with conducting outer layers

The origin of the coordinate system is located at the bottom of the composite layer with $\hat{x}$ and $\hat{y}$ being the horizontal coordinates and $\hat{z}$, the vertical coordinate. Dirichlet conditions for temperature are applied at the external surfaces of the composite layer, i.e. at $\hat{z} = 0$ and at $\hat{z} = h_1 + h_2 + h_3$.

The full governing equations for the porous layer are

$$\frac{\partial \hat{u}}{\partial \hat{x}} + \frac{\partial \hat{v}}{\partial \hat{y}} + \frac{\partial \hat{w}}{\partial \hat{z}} = 0, \tag{1}$$

$$\hat{u} = -\frac{K}{\mu}\frac{\partial \hat{p}}{\partial \hat{x}}, \qquad \hat{v} = -\frac{K}{\mu}\frac{\partial \hat{p}}{\partial \hat{y}}, \qquad \hat{w} = -\frac{K}{\mu}\frac{\partial \hat{p}}{\partial \hat{z}} + \frac{\rho_2 \bar{g}\beta K}{\mu}(T_2 - T_{\text{ref}}), \tag{2}$$

$$(\rho C)_2 \frac{\partial T_2}{\partial t} + (\rho C)_{\text{f}}\left(\hat{u}\frac{\partial T_2}{\partial \hat{x}} + \hat{v}\frac{\partial T_2}{\partial \hat{y}} + \hat{w}\frac{\partial T_2}{\partial \hat{z}}\right) = k_2\left(\frac{\partial^2 T_2}{\partial \hat{x}^2} + \frac{\partial^2 T_2}{\partial \hat{y}^2} + \frac{\partial^2 T_2}{\partial \hat{z}^2}\right), \tag{3}$$

where all quantities are given in the "List of Symbols". The respective equations for conductive heat transfer in the lower and upper impermeable layers are,

$$(\rho C)_1 \frac{\partial T_1}{\partial \hat{t}} = k_1\left(\frac{\partial^2 T_1}{\partial \hat{x}^2} + \frac{\partial^2 T_1}{\partial \hat{y}^2} + \frac{\partial^2 T_1}{\partial \hat{z}^2}\right), \tag{4}$$

and

$$(\rho C)_3 \frac{\partial T_3}{\partial \hat{t}} = k_3\left(\frac{\partial^2 T_3}{\partial \hat{x}^2} + \frac{\partial^2 T_3}{\partial \hat{y}^2} + \frac{\partial^2 T_3}{\partial \hat{z}^2}\right). \tag{5}$$

In these equations the numerical subscripts refer to the appropriate sublayer. The boundary and interface conditions are,

$$\begin{aligned}
&\hat{z} = 0: \quad T_1 = T_{\text{ref}},\\
&\hat{z} = h_1: \quad \hat{w} = 0, \quad T_1 = T_2, \quad k_1\frac{\partial T_1}{\partial \hat{z}} = k_2\frac{\partial T_2}{\partial \hat{z}},\\
&\hat{z} = h_1 + h_2: \quad \hat{w} = 0, \quad T_2 = T_3, \quad k_2\frac{\partial T_2}{\partial \hat{z}} = k_3\frac{\partial T_3}{\partial \hat{z}},\\
&\hat{z} = h_1 + h_2 + h_3: \quad T_3 = -\frac{k_2}{h_2}\Delta T\left(\frac{h_1}{k_1} + \frac{h_2}{k_2} + \frac{h_3}{k_3}\right) + T_{\text{ref}}.
\end{aligned} \tag{6}$$

The reason for such an unusual expression for the imposed temperature at the upper surface is that it guarantees that the temperature change over the porous layer is precisely ΔT, and it is this quantity that will be used for nondimensionalisation purposes.

We may now make the governing equations nondimensional by introducing the following scalings,

$$(\hat{x}, \hat{y}, \hat{z}) = (0, 0, h_1) + h_2(x, y, z), \qquad \hat{t} = \frac{h_2^2(\rho C)_2}{k_2} t, \qquad \hat{p} = \frac{k_2 \mu}{(\rho C)_{\mathrm{f}} K} p,$$
$$(\hat{u}, \hat{v}, \hat{w}) = \frac{k_2}{h_2(\rho C)_{\mathrm{f}}}(u, v, w), \qquad T = T_{\mathrm{ref}} - \frac{k_2}{k_1}\frac{h_1}{h_2}\Delta T + \Delta T\, \theta, \tag{7}$$

which are based on the height and the properties of the porous layer.

The nondimensional equations are now,

$$\frac{\partial u}{\partial x} + \frac{\partial v}{\partial y} + \frac{\partial w}{\partial z} = 0, \tag{8}$$

$$u = -\frac{\partial p}{\partial x}, \quad v = -\frac{\partial p}{\partial y}, \quad w = -\frac{\partial p}{\partial z} + Ra\, \theta_2, \tag{9}$$

$$\frac{\partial \theta_2}{\partial t} + u\frac{\partial \theta_2}{\partial x} + v\frac{\partial \theta_2}{\partial y} + w\frac{\partial \theta_2}{\partial z} = \frac{\partial^2 \theta_2}{\partial x^2} + \frac{\partial^2 \theta_2}{\partial y^2} + \frac{\partial^2 \theta_2}{\partial z^2}, \tag{10}$$

$$\frac{\partial \theta_1}{\partial t} = \kappa_1 \left(\frac{\partial^2 \theta_1}{\partial x^2} + \frac{\partial^2 \theta_1}{\partial y^2} + \frac{\partial^2 \theta_1}{\partial z^2} \right), \tag{11}$$

and

$$\frac{\partial \theta_3}{\partial t} = \kappa_3 \left(\frac{\partial^2 \theta_3}{\partial x^2} + \frac{\partial^2 \theta_3}{\partial y^2} + \frac{\partial^2 \theta_3}{\partial z^2} \right). \tag{12}$$

The diffusivity ratios, κ_1 and κ_3, are defined according to,

$$\kappa_1 = \frac{k_1(\rho C)_2}{k_2(\rho C)_1}, \qquad \kappa_3 = \frac{k_3(\rho C)_2}{k_2(\rho C)_3}, \tag{13}$$

and these play a significant role only when one is interested in unsteady convection. The Darcy–Rayleigh number is defined to be,

$$Ra = \frac{\rho_2(\rho C)_{\mathrm{f}} \bar{g} \beta h_2 K \Delta T}{\mu k_2}, \tag{14}$$

and it is based upon the height of the porous layer and the temperature difference across it, rather than upon the corresponding properties of the full composite system.

We may also define two conductivity ratios and two thickness ratios as follows,

$$d_1 = k_1/k_2, \quad d_3 = k_3/k_2, \quad \delta_1 = h_1/h_2, \quad \delta_3 = h_3/h_2. \tag{15}$$

Thus, while unsteady nonlinear convection depends on the values of seven parameters (Ra, κ_1, κ_3, d_1, d_3, δ_1 and δ_3), the determination of the onset of convection itself relies on only four (d_1, d_3, δ_1 and δ_3) since the onset is steady and Ra is computed rather than imposed.

The boundary and interface conditions now become

$$\begin{aligned} z = -\delta_1: &\quad \theta_1 = \delta_1/d_1, \\ z = 0: &\quad \frac{\partial p}{\partial z} = Ra\,\theta_2, \quad \theta_1 = \theta_2, \quad d_1\frac{\partial \theta_1}{\partial z} = \frac{\partial \theta_2}{\partial z}, \\ z = 1: &\quad \frac{\partial p}{\partial z} = Ra\,\theta_2, \quad \theta_2 = \theta_3, \quad d_3\frac{\partial \theta_3}{\partial z} = \frac{\partial \theta_2}{\partial z}, \\ z = 1+\delta_3: &\quad \theta_3 = -1 - \delta_3/d_3. \end{aligned} \tag{16}$$

Given that we seek to determine whether three-dimensional modes are realisable, we will adopt a pressure/temperature formulation of the equation for flow in the porous layer. On eliminating the velocities between Eqs. 8 and 9 we obtain the following momentum equation,

$$\nabla^2 p = Ra\,\frac{\partial \theta_2}{\partial z}, \tag{17}$$

while the heat transport equation becomes,

$$\frac{\partial \theta_2}{\partial t} = \nabla^2\theta_2 + \frac{\partial p}{\partial x}\frac{\partial \theta_2}{\partial x} + \frac{\partial p}{\partial y}\frac{\partial \theta_2}{\partial y} + \left(\frac{\partial p}{\partial z} - Ra\,\theta_2\right)\frac{\partial \theta_2}{\partial z}. \tag{18}$$

The basic state whose stability characteristics we seek is given by

$$\theta_1 = -z/d_1, \qquad \theta_2 = -z, \qquad \theta_3 = -1 - (z-1)/d_3, \qquad p = -Ra\,z^2/2. \tag{19}$$

Of interest is the fact that, θ_2, the temperature distribution within the porous layer, is independent of the governing nondimensional parameters. This is a consequence of the fact that we have taken the temperature difference across the porous layer to be the reference temperature scale when defining the Darcy–Rayleigh number, Ra.

3 Linear Stability Analysis

The present configuration is different from that of Mojtabi and Rees (2011), who considered constant heat flux conditions at both of the outer surfaces, because we have taken fixed temperature conditions. Further, Mojtabi and Rees (2011) confined their attention to cases where the two bounding plates are identical in all respects. Therefore, it is essential to summarise briefly the appropriate linear theory for the present situation before developing the weakly nonlinear analysis.

On subtracting the basic state, which is given by Eq. 19, from the governing equations, Eqs. 11, 12, 17 and 18, the full system governing the evolution of perturbations is found to be,

$$\kappa_1\nabla^2\theta_1 = \frac{\partial \theta_1}{\partial t}, \tag{20}$$

$$\kappa_3\nabla^2\theta_3 = \frac{\partial \theta_3}{\partial t}, \tag{21}$$

$$\nabla^2 p - Ra\,\frac{\partial \theta_2}{\partial z} = 0, \tag{22}$$

$$\nabla\theta_2 + Ra\,\theta_2 - \frac{\partial p}{\partial z} = \frac{\partial \theta_2}{\partial t} - \nabla p\cdot\nabla\theta_2 + Ra\,\theta_2\frac{\partial \theta_2}{\partial z}, \tag{23}$$

where these equations have been written in such a way that the replacement of all the right hand sides by zero will yield the equations governing the onset of stationary modes.

We may Fourier-decompose the linearised equations using the following substitutions,

$$(\theta_1, \theta_2, \theta_3, p) = \left(\tilde{\theta_1}, \tilde{\theta_2}, \tilde{\theta_3}, \tilde{p}\right) e^{i\alpha x} + \text{c.c.}, \tag{24}$$

where all quantities with the tilde are functions of the vertical coordinate, z, only. We obtain the following ordinary differential eigenvalue problem for the Darcy–Rayleigh number in terms of the wavenumber, α:

$$\begin{aligned} &\tilde{\theta_1}'' - \alpha^2 \tilde{\theta_1} = 0, \quad \tilde{\theta_2}'' + (Ra - \alpha^2)\tilde{\theta_2} - \tilde{p}' = 0, \\ &\tilde{\theta_3}'' - \alpha^2 \tilde{\theta_3} = 0, \quad \tilde{p}'' - \alpha^2 \tilde{p} - Ra\, \tilde{\theta_2}' = 0, \end{aligned} \tag{25}$$

where primes denote derivatives with respect to z.

The general solution for $\tilde{\theta_1}$ in the lower layer and which is zero at $z = -\delta_1$ is,

$$\tilde{\theta_1} = \mathcal{A} \sinh \alpha(z + \delta_1), \tag{26}$$

where the constant, $\mathcal{A}$, is arbitrary. However, at the interface at $z = 0$, it is necessary to apply the interface conditions that $\tilde{\theta_1} = \tilde{\theta_2}$ and $d_1 \tilde{\theta_1}' = \tilde{\theta_2}$. This process yields the following values for $\tilde{\theta_2}$ and $\tilde{\theta_2'}$ at $z = 0$,

$$\tilde{\theta_2} = \mathcal{A} \sinh \alpha\delta_1, \qquad \tilde{\theta_2}' = \mathcal{A} d_1 \alpha \cosh \alpha\delta_1. \tag{27}$$

The constant, $\mathcal{A}$, may now be eliminated to yield the following mixed boundary condition which effectively replaces the presence of the lower layer when solutions are stationary:

$$\tilde{\theta_2}' = [d_1 \alpha \coth \alpha\delta_1]\, \theta_2 \quad \text{at} \quad z = 0. \tag{28}$$

A similar analysis for the upper layer results in the equivalent formula,

$$\tilde{\theta_2}' = -[d_3 \alpha \coth \alpha\delta_3]\, \theta_2 \quad \text{at} \quad z = 1. \tag{29}$$

We note that neither Eq. 28 nor Eq. 29 is a conventional boundary condition of the third kind (i.e. a Robin condition), such as is represented by Newton's law of cooling, because the relationship between the temperature and the temperature gradient depends on the wavenumber, α, and hence on the depth of penetration of the thermal field into the conducting layers. We also note that we obtain the boundary conditions presented in Riahi (1983) if we allow both δ_1 and δ_3 to become infinitely large, which is equivalent to having vertically unbounded conducting domains above and below the porous layer.

The solution in the porous layer may now be obtained by expanding $\tilde{\theta_2}$ and p in terms of eigenfunctions, and by applying the new mixed boundary conditions for $\tilde{\theta_2}$, namely, Eqs. 28 and 29, and those for pressure, namely, $\tilde{p}' = Ra\, \tilde{\theta_2}$ at $z = 0, 1$. The process is straightforward but lengthy, and it eventually yields the following dispersion relation relating Ra and α:

$$\begin{aligned} &\alpha^2 \sin\sigma \sinh\lambda \,(1 + d_1 d_3 \coth\alpha\delta_1 \coth\alpha\delta_3) + \lambda\sigma \,(\cos\sigma \cosh\lambda - 1) \\ &+\alpha \,(d_1 \coth\alpha\delta_1 + d_3 \coth\alpha\delta_3)\,(\sigma \cos\sigma \sinh\lambda + \lambda \cosh\lambda \sin\sigma) = 0, \end{aligned} \tag{30}$$

where

$$\lambda^2 = \alpha Ra^{1/2} + \alpha^2, \qquad \sigma^2 = \alpha Ra^{1/2} - \alpha^2. \tag{31}$$

The corresponding dispersion relation for the case of constant heat flux boundary conditions at the outer surfaces of the composite layer is obtained by simply replacing the hyperbolic cotangents by hyperbolic tangents, and this new formula agrees with that obtained by Mojtabi and Rees (2011) on setting $\delta_1 = \delta_3 \equiv \delta$ and $d_1 = d_3 \equiv d$.

It appears that all the neutral curves have unimodal form and each has a well-defined and unique minimum. Such minima were obtained using a simple Newton-Raphson procedure, as follows. If we rewrite the dispersion relation, (30), in the form, $\mathcal{F}(Ra, \alpha) = 0$, then the minimum in the neutral curve corresponds to needing both

$$\mathcal{F} = 0 \qquad \text{and} \qquad \frac{\partial \mathcal{F}}{\partial \alpha} = 0 \tag{32}$$

to be satisfied simultaneously. The iteration scheme is,

$$\begin{pmatrix} Ra_{m+1} \\ \alpha_{m+1} \end{pmatrix} = \begin{pmatrix} Ra_m \\ \alpha_m \end{pmatrix} - \begin{pmatrix} \dfrac{\partial \mathcal{F}}{\partial Ra} & \dfrac{\partial^2 \mathcal{F}}{\partial Ra \partial \alpha} \\ \dfrac{\partial \mathcal{F}}{\partial \alpha} & \dfrac{\partial^2 \mathcal{F}}{\partial \alpha^2} \end{pmatrix}^{-1} \begin{pmatrix} \mathcal{F} \\ \dfrac{\partial \mathcal{F}}{\partial \alpha} \end{pmatrix}, \tag{33}$$

where the subscript, m, denotes the iteration number. The partial derivatives were evaluated using numerical differentiation, and the solutions obtained for Ra and α are correct to more than six decimal places in all cases.

4 Onset Criteria

Although it is impossible to check over the whole of the four-dimensional parameter space spanned by the nondimensional parameters, δ_1, δ_3, d_1 and d_3, we believe it to be true that the neutral curve governing the onset of convection takes its classical form, namely that it has a single minimum, and that $Ra \to \infty$ when $\alpha \to 0$ and when $\alpha \to \infty$. Therefore, we focus our interest on the values of Ra and α at the minimum of the neutral curve, and these are denoted by Ra_c and α_c, respectively.

Figure 2 summarises the onset criteria for symmetric configurations where the bounding layers are identical. For the present purpose we define $\delta = \delta_1 = \delta_3$ and $d = d_1 = d_3$. It is very clear from this figure and the numerical data used in its preparation that we recover the classical Darcy–Bénard stability criterion when d is sufficiently large and that of its constant heat flux analogue when d is sufficiently small. Thus, we have

$$\lim_{d\to\infty} (Ra_c, k_c) = (4\pi^2, \pi) \quad \text{and} \quad \lim_{d\to 0} (Ra_c, k_c) = (12, 0). \tag{34}$$

From the physical point of view the limiting case, $d \to \infty$, corresponds to perfectly conducting bounding layers, and hence temperature perturbations within the porous layer do not penetrate into the bounding layers. When $d \to 0$ the heat flux is not affected by the x-variation of the temperature at the boundaries of the porous layer. Thus, the effective boundary conditions for the porous layer correspond to the constant heat flux case; see Eqs. 28 and 29.

These conclusions may also be drawn from the dispersion relation given in Eq. 30. When d is large, a formal large-d expansion will yield $\sin \sigma = 0$ at leading order. Given the definition of σ in Eq. 31, this condition is equivalent to

$$Ra = \frac{(n^2\pi^2 + \alpha^2)^2}{\alpha^2}, \tag{35}$$

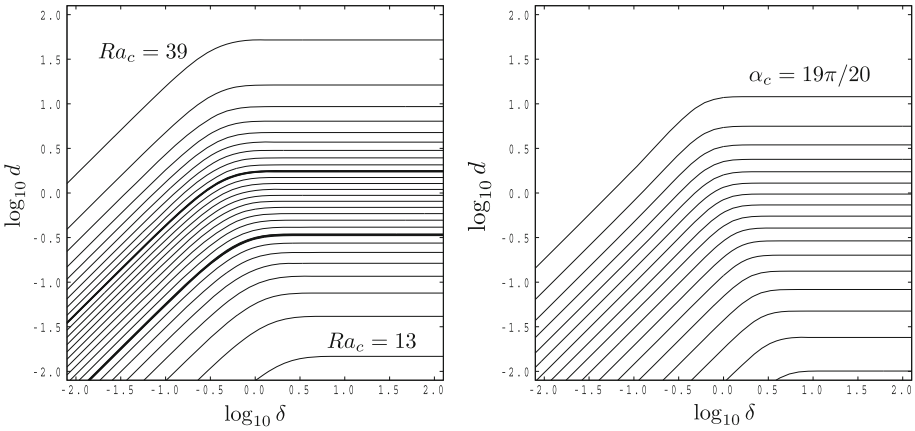

Fig. 2 Displaying contours of Ra_c and α_c as functions of δ and d for symmetric bounding sublayers. The contours of Ra_c and α_c are in intervals of 1 and $\pi/20$, respectively, and values decrease downwards. The $Ra_c = 20$ and 30 contours correspond to *thick lines*

where $n = 1$ yields the first mode. On the other hand, when $d \to 0$, then the dispersion relation in Eq. 30 reduces to

$$\alpha^2 \sin\sigma \sinh\lambda + \lambda\sigma \left(\cos\sigma \cosh\lambda - 1\right), \tag{36}$$

which is identical to the relation given in Rees and Genç (2011) for the constant heat flux form of the Darcy–Bénard problem.

We also note that the classical Darcy–Bénard criteria are also recovered when $\delta \to 0$, and a similar argument based upon the dispersion relation may be made to show this. Physically, however, this limit corresponds to vanishingly thin bounding layers.

Figures 3 and 4 summarise the onset criteria for asymmetric cases. In all the cases presented the top right-hand corner of the frames correspond to the classical Darcy–Bénard problem, while the bottom left-hand corner corresponds to the constant heat flux analogue. The remaining two corners are equivalent to having one porous boundary with a Dirichlet boundary condition and the other with Neumann boundary condition. Thus these corners correspond to $Ra_c \to 27.097628$ and $\alpha_c \to 2.326215$ as either $d_1 \to \infty$ and $d_3 \to 0$ or $d_1 \to 0$ and $d_3 \to \infty$.

In Fig. 3 we retain the fact that the bounding layers have identical thicknesses, but we assess the effect of having different conductivities in these layers. The first case shown corresponds to $\delta = 1$, and therefore the bounding layers have the same thickness as the central porous layer. The transition between the three asymptotic cases mentioned above is seen clearly, and we note that the shape of the isolines of both Ra_c and α_c when $\delta = 1$ are found not to alter significantly as δ varies, although the location of the pattern relative to the origin does vary. However, we note that the $\delta = 1$ case also represents very accurately those cases for which δ takes larger values. On the other hand, when δ takes successively smaller values, it appears that the isolines move by a corresponding factor, as depicted by the comparison between the $\delta = 0.1$ and $\delta = 0.01$ cases. Thus, for small values of δ the isolines, when drawn as a function of $\log_{10}(d_1/\delta)$ and $\log_{10}(d_3/\delta)$, do not vary with δ.

This small-δ similarity solution may also have been predicted by setting $d_i = \gamma_i \delta$ (for $i = 1, 3$) in the dispersion relation, Eq. 30. Thus, we obtain the following version of the dispersion relation when$\delta_1 = \delta_3 \equiv \delta$:

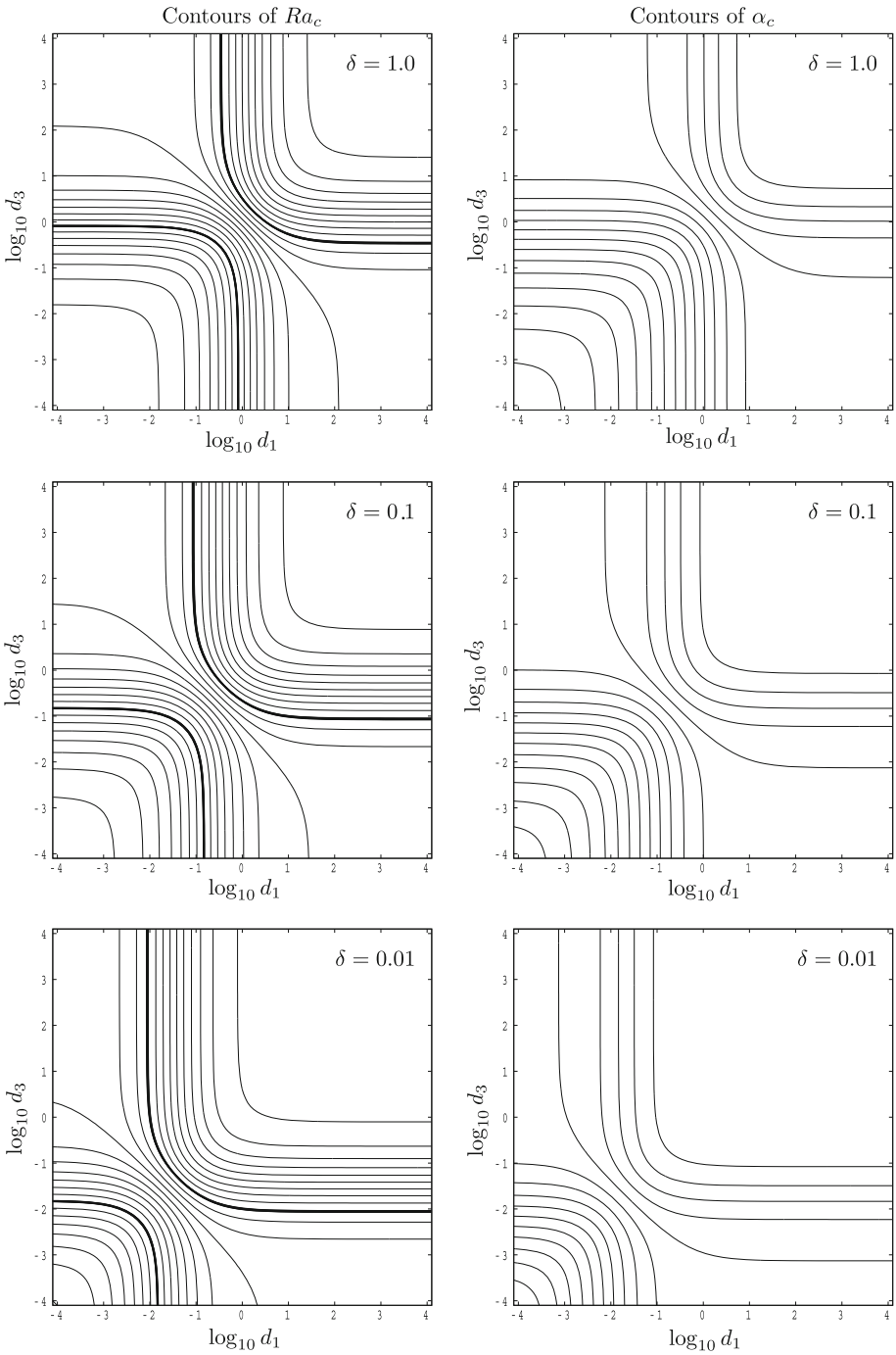

Fig. 3 Displaying contours of Ra_c and α_c as functions of d_1 and d_3 for $\delta = 1,\ 0.1$ and 0.01. Contour levels are as described in Fig. 2. In all cases $Ra_c \sim 4\pi^2$ and $\alpha_c \sim \pi$ in the *top right-hand corners* of the frames, while $Ra_c \sim 12$ and $\alpha_c \sim 0$ in the *bottom left-hand corners*

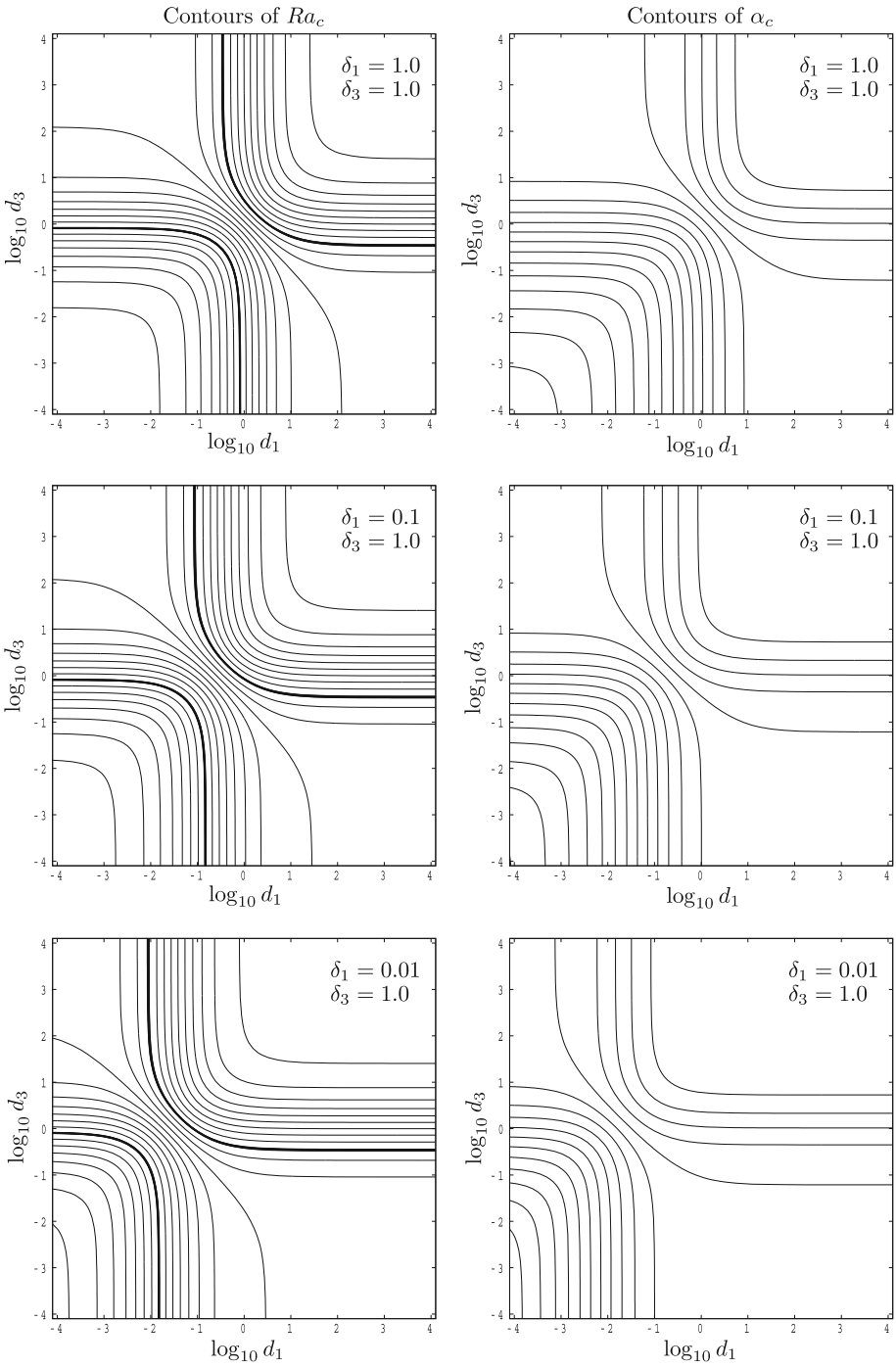

Fig. 4 Displaying contours of Ra_c and α_c as functions of d_1 and d_3 for $\delta_3 = 1,\ 0.1$ and 0.01 with $\delta_1 = 1$. Contour levels are as described in Fig. 2. In all cases $Ra_c \sim 4\pi^2$ and $\alpha_c \sim \pi$ in the *top right-hand corners* of the frames, while $Ra_c \sim 12$ and $\alpha_c \sim 0$ in the *bottom left-hand corners*

$$\alpha^2 \sin\sigma \sinh\lambda \left(1 + \delta^2 \gamma_1 \gamma_3 \coth^2 \alpha\delta\right) + \lambda\sigma \left(\cos\sigma \cosh\lambda - 1\right)$$
$$+\alpha\delta(\gamma_1 + \gamma_3) \coth\alpha\delta \left(\sigma \cos\sigma \sinh\lambda + \lambda \cosh\lambda \sin\sigma\right) = 0. \tag{37}$$

If we now let $\delta \to 0$ and retain only the leading order behaviour of the hyperbolic cotangent terms, then the relation reduces further to,

$$\alpha^2 \sin\sigma \sinh\lambda \left(1 + \frac{\gamma_1\gamma_3}{\alpha^2}\right) + \lambda\sigma \left(\cos\sigma \cosh\lambda - 1\right)$$
$$+(\gamma_1 + \gamma_3) \left(\sigma \cos\sigma \sinh\lambda + \lambda \cosh\lambda \sin\sigma\right) = 0, \tag{38}$$

where the largest term that has been neglected is of $O(\delta^2)$. Therefore, we conclude that the shapes taken by the isolines are independent of δ when δ is small and when they are plotted in terms of d_1/δ and d_3/δ.

It is possible to make similar observations about Fig. 4, which shows corresponding isolines when δ_1 varies but where δ_3 is held fixed at a unit value. For these cases we may say (i) the locations of the isolines shown in the $\delta_1 = \delta_3 = 1$ frames are not changed by an increase in either δ_1 or δ_3, and (ii) when δ_1 is small, then the corresponding isolines are independent of δ_1 when drawn as a function of $\log_{10}(d_1/\delta_1)$.

5 Weakly Nonlinear Analysis

The above linear theory assumes that disturbances take the form of two-dimensional rolls. However, rolls of other orientations may be added to any one such roll to obtain different convection patterns. Thus, the addition of two rolls at right angles will form a square cell pattern, when viewed from above, when the rolls have identical amplitude, while the superposition of three rolls at 60° relative orientation yields a hexagonal pattern. Competition between these patterns under slightly supercritical conditions may be determined using weakly nonlinear theory. Following the style of analysis introduced in Newell and Whitehead (1969) and given in more detail in the context of Darcy–Bénard convection in Rees (2001), we will expand the solutions to Eqs. 22 and 23 in a suitable power series. However, we need to avoid a potential clash of notation in this section of the paper, and therefore, from this point forward, we will replace θ_2 by Θ, so that successive terms in the weakly nonlinear expansion may be identified by their subscripts.

The weakly nonlinear expansion takes the following form,

$$\begin{pmatrix} p \\ \Theta \end{pmatrix} = \epsilon \begin{pmatrix} p_1 \\ \Theta_1 \end{pmatrix} + \epsilon^2 \begin{pmatrix} p_2 \\ \Theta_2 \end{pmatrix} + \epsilon^3 \begin{pmatrix} p_3 \\ \Theta_3 \end{pmatrix} + \cdots, \tag{39}$$

where the small quantity, ϵ, is defined according to,

$$Ra = Ra_0 + \epsilon^2 Ra_2 + \cdots. \tag{40}$$

In the above, Ra_0 is an alternative notation for the critical Darcy–Rayleigh number, Ra_c, and slightly supercritical conditions are equivalent to positive $O(1)$ values of Ra_2. At successive orders of expansion we obtain the following systems, in turn.

At $O(\epsilon)$:

$$\nabla^2 p_1 - Ra_0 \frac{\partial\Theta_1}{\partial z} = 0, \tag{41}$$

$$\nabla^2 \Theta_1 + Ra_0 \Theta_1 - \frac{\partial p_1}{\partial z} = 0. \tag{42}$$

At $O(\epsilon^2)$:

$$\nabla^2 p_2 - Ra_0 \frac{\partial \Theta_2}{\partial z} = 0, \tag{43}$$

$$\nabla^2 \Theta_2 + Ra_0 \Theta_2 - \frac{\partial p_2}{\partial z} = Ra_0 \Theta_1 \frac{\partial \Theta_1}{\partial z} - \nabla p_1 \cdot \nabla \Theta_1. \tag{44}$$

At $O(\epsilon^3)$:

$$\nabla^2 p_3 - Ra_0 \frac{\partial \Theta_3}{\partial z} = Ra_2 \frac{\partial \Theta_1}{\partial z}, \tag{45}$$

$$\begin{aligned} \nabla^2 \Theta_3 + Ra_0 \Theta_3 - \frac{\partial p_3}{\partial z} &= Ra_0 \left(\Theta_1 \frac{\partial \Theta_2}{\partial z} + \Theta_2 \frac{\partial \Theta_1}{\partial z} \right) \\ &\quad - \nabla p_1 \cdot \nabla \Theta_2 - \nabla p_2 \cdot \nabla \Theta_1 + \frac{\partial \Theta_1}{\partial \tau} - Ra_2 \Theta_1. \end{aligned} \tag{46}$$

In the above, $\tau = \epsilon^2 t$, is a slow timescale.

Further details on how these equations have been solved are given in the Appendix, but it is important to note that the $O(\epsilon)$ equations are identical to the linearised stability equations presented earlier. We assume that the solution takes the form of two rolls of relative orientation, ϕ. More specifically, the solutions are of the form,

$$\begin{aligned} \begin{pmatrix} p_1 \\ \Theta_1 \end{pmatrix} = & \begin{pmatrix} f_1(z) \\ g_1(z) \end{pmatrix} \left[A e^{i\alpha x} + \overline{A} e^{-i\alpha x} \right] \\ & + \begin{pmatrix} f_1(z) \\ g_1(z) \end{pmatrix} \left[B e^{i\alpha (x \cos\phi - y \sin\phi)} + \overline{B} e^{-i\alpha (x \cos\phi - y \sin\phi)} \right], \end{aligned} \tag{47}$$

where the modal amplitudes, A and B, are functions only of the slow time scale, τ. The inhomogeneous terms in the third-order equations, (45) and (46), contain terms which have components of the form of the first-order eigenmodes. However, the value of Ra_2 may be chosen to ensure that the these components become nonresonant, i.e. are orthogonal to the eigensolution. Application of the appropriate solvability conditions yield the following pair of amplitude equations,

$$c_1 \frac{\partial A}{\partial \tau} = Ra_2 A - A \left(c_2 A \overline{A} + c_3 B \overline{B} \right), \tag{48}$$

$$c_1 \frac{\partial B}{\partial \tau} = Ra_2 B - B \left(c_2 B \overline{B} + c_3 A \overline{A} \right). \tag{49}$$

The values of c_1, c_2 and c_3 always take positive values, and the value of c_1 also depends on the diffusivity ratios, κ_1 and κ_3. It is to be expected that c_1 should be positive because it means that growth of the disturbances take place only when $Ra_2 > 0$, i.e. when the Darcy–Rayleigh number is above its critical value. The positive of value c_2 means that the onset of convection is supercritical. The value of c_3 also depends on the relative orientation of the two roll solutions. In all the cases we tried, c_3 takes its smallest value when the rolls are perpendicular to one another. The detailed analysis of Rees and Riley (1990) shows that the identity of the postcritical pattern depends on the minimum value of the ratio,

$$\Omega(\phi) = c_3 / c_2. \tag{50}$$

For the classical Darcy–Bénard problem, Rees and Riley (1989a) showed that,

$$\Omega = \frac{70 + 28 \cos^2\phi - 2 \cos^4\phi}{49 - 2 \cos^2\phi + \cos^4\phi}, \tag{51}$$

which varies between the maximum of 2 when $\phi = 0$ and the minimum of $10/7$ when $\phi = \pm\frac{1}{2}\pi$. However, values of Ω need to be computed for more complicated configurations, such as the present one.

When $\min_\phi \Omega(\phi) > 1$, then rolls are stable and square cells are unstable to perturbations of the form of one of the constituent rolls. In such situations rolls also transport more heat than do square cells (Rees 2001). The situation is reversed in all respects when $\min_\phi \Omega < 1$ and square cells then form the stable pattern.

6 Weakly Nonlinear Results

Although the computations for the linearised theory employed the Newton–Raphson method to solve the dispersion relation, the governing ordinary differential equations for the weakly nonlinear theory were solved using a shooting method algorithm together with a fourth-order Runge–Kutta method. Initial conditions for the $O(\epsilon)$ equations were given by the dispersion relation analysis, while the fact that the second and third-order equations are linear meant that the initial iterate for the unknown initial conditions could be set to zero. We used 100 intervals in the range $0 \le z \le 1$, and the presence of the bounding layers are modelled by means of appropriate boundary conditions; see Eqs. 57 and 58 in the Appendix.

The sole aim of this section is to determine regions in parameter space wherein either rolls are stable or square cells are stable. The simplest way of doing this was to choose two parameters to be fixed and two to vary from the set of four. Given that Riahi (1983) varied the conductivity ratios we have done the same, so that some comparison may be made. Thus, for a chosen pair of values of δ_1 and δ_3 the condition $\Omega(\frac{1}{2}\pi) = 1$ maps out a curve in (d_1, d_3)-space. The curve was found by calculating the values of $\Omega(\frac{1}{2}\pi)$ on a fine grid of values of d_1 and d_3 and then by drawing the $\Omega = 1$ contour.

Figure 5 shows the $\Omega(\frac{1}{2}\pi) = 1$ contours for various cases for which $\delta_1 = \delta_3 \equiv \delta$. For each case shown, the region which includes the origin is the one within which square cells are stable. The curve marked $\delta \gg 1$ corresponds to the case computed by Riahi (1983), and the agreement is excellent.

As δ decreases, which corresponds to bounding layers of decreasing thicknesses, the size of the square-cell region also decreases, and shrinks towards the origin. For small values of δ the figure suggests the rate of shrinking is proportional to the magnitude of δ, and therefore that there may again be a simple scaling for d_1 and d_3 in terms of δ. Such an asymptotic analysis is now extremely complicated because it would require the solution of all the equations given in the Appendix. Therefore, we performed a numerical investigation by displaying the contours of $\Omega(\frac{1}{2}\pi) = 1$ as functions of d_1/δ and d_3/δ; these are shown in Fig. 6.

Figure 6 suggests very strongly that there is well-defined limiting contour of $\Omega(\frac{1}{2}\pi) = 1$ as $\delta \to 0$ when plotted in $(d_1/\delta, d_3/\delta)$-coordinates. We may also make the following two observations. First, if the bounding layers are less than 10% of the thickness of the porous layer (i.e. $\delta < 0.1$), then square cells are preferred if both the conditions, $d_1 < 0.9\delta$ and $d_3 < 0.9\delta$, are satisfied. This is, of course, a fairly crude condition, because square cells are preferred in a much larger domain than this, but it is a useful rule-of-thumb. Second, it is clear that, for any chosen value of δ, the small d_1 and d_3 limits correspond to square convective planforms. These limits are equivalent to the constant heat flux analogue of the Darcy–Bénard problem, for which $Ra_c \sim 12$ and $\alpha_c \sim 0$.

Figures 7 and 8 show how the $\Omega < 1$ square cell domain varies with δ_3 when δ_1 takes fixed values. Figure 7 corresponds to $\delta_1 = 1$ while Fig. 8 has $\delta_1 = 0.3$; the figures are drawn

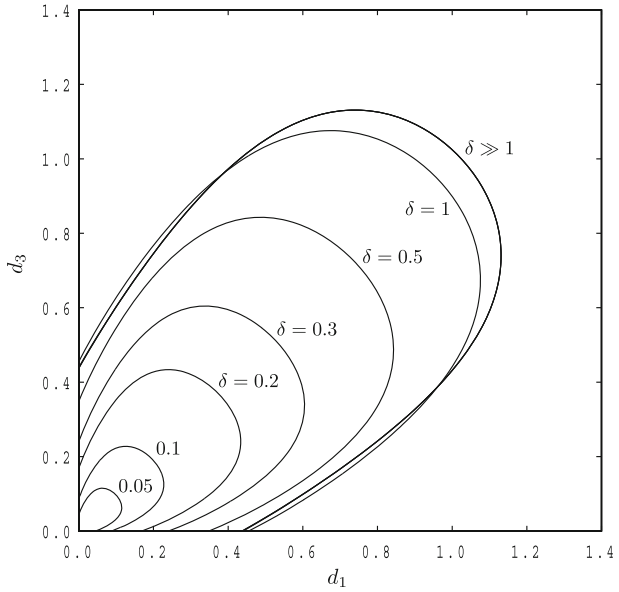

Fig. 5 Displaying contours of $\Omega(\pi/2) = 1$ in (d_1, d_3)-space for $\delta = 0.05,\ 0.1,\ 0.2,\ 0.3,\ 0.5$ and 1.0, and as $\delta \to \infty$. The region containing the origin corresponds to where square cells are favoured

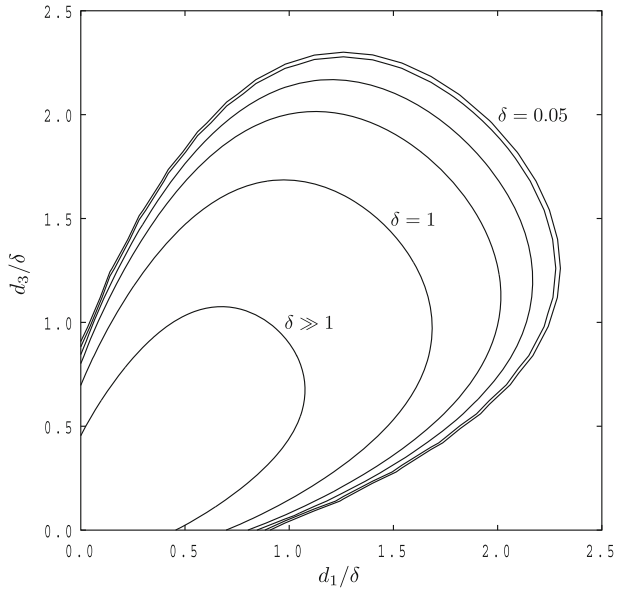

Fig. 6 Displaying contours of $\Omega(\pi/2) = 1$ in $(d_1/\delta, d_3/\delta)$-space for $\delta = 0.05,\ 0.1,\ 0.2,\ 0.3,\ 0.5$ and 1.0, and as $\delta \to \infty$. The region containing the origin corresponds to where square cells are favoured

to the same scale to aid comparison. The chief difference between these figures and Fig. 5 is that range of the square-cell domain in the d_1-direction is almost independent of δ_3, although the size of the domain in the d_3-direction is strongly dependent on it.

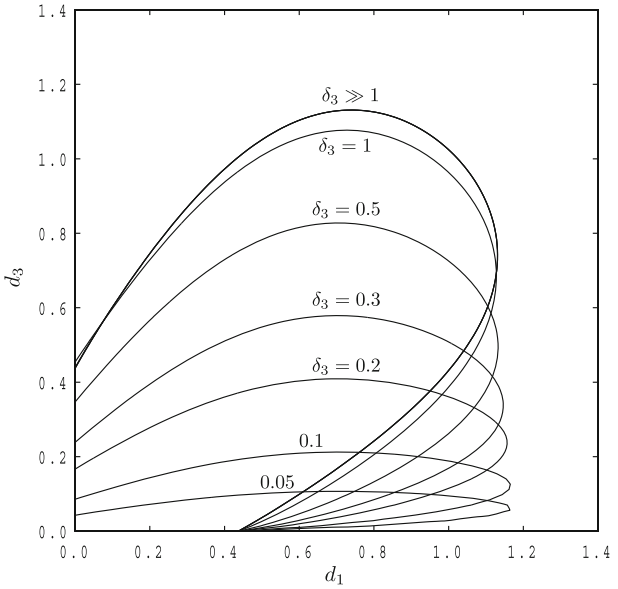

Fig. 7 Displaying contours of $\Omega(\pi/2) = 1$ in (d_1, d_3)-space for $\delta_3 = 0.05,\ 0.1,\ 0.2,\ 0.3,\ 0.5$ and 1.0, and as $\delta_3 \to \infty$ and with $\delta_1 = 1$. The region containing the origin corresponds to where square cells are favoured

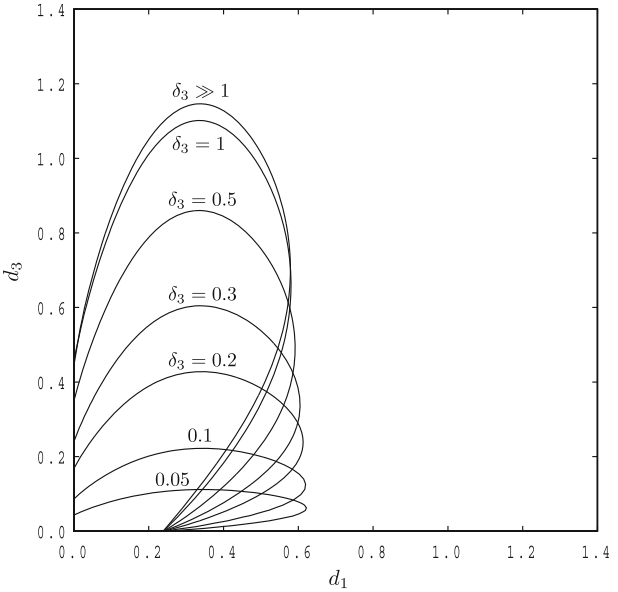

Fig. 8 Displaying contours of $\Omega(\pi/2) = 1$ in (d_1, d_3)-space for $\delta_3 = 0.05,\ 0.1,\ 0.2,\ 0.3,\ 0.5$ and 1.0, and as $\delta_3 \to \infty$ and with $\delta_1 = 0.3$. The region containing the origin corresponds to where square cells are favoured

7 Final Remarks

In this paper we have considered the effect of conducting bounding plates on the onset of convection and the identity of the preferred weakly postcritical convection planform. The

linear theory was carried out using an analysis based upon the dispersion relation, while the weakly nonlinear analysis used a highly accurate Runge–Kutta scheme. We have been able to identify very strong patterns in the behaviour of Ra_c and α_c as the governing parameters change, and much of this has been explained in physical terms and by means of further analysis of the dispersion relation. With regard to weakly nonlinear convection, our analysis suggests strongly that, for any chosen thicknesses of the bounding layers, there is always a region of (d_1, d_3)-space within which square cells are preferred. Further, if may be inferred from our analysis that the constant heat flux analogue of the classical Darcy–Bénard problem also admits square-cell convection patterns immediately post onset; as far as we are aware this is a new finding.

Acknowledgment The first author (D.A.S.R.) wishes to thank the Université Paul Sabatier, Toulouse, France, for funding a visiting professorship which enabled this work to be carried out.

Appendix

In this Appendix we present the equations and boundary conditions that need to be solved in order to find the coefficients in the amplitude equations. A fourth-order Runge–Kutta scheme allied with a user-written, but near-black-box shooting method code was used to solve all the ordinary differential equations which arise. The use of 100 intervals coupled with the order of accuracy resulted in solutions of at least six decimal places.

Modal interactions of the first-order solutions mean that the following substitutions need to be made to solve the second-order equations:

$$\begin{aligned}\begin{pmatrix} p_2 \\ \Theta_2 \end{pmatrix} = &\begin{pmatrix} f_2(z) \\ g_2(z) \end{pmatrix}\left[A^2 e^{2i\alpha x} + \text{c.c.} + B^2 e^{2i\alpha(x\cos\phi - y\sin\phi)} + \text{c.c.}\right] \\ &+ \begin{pmatrix} f_0(z) \\ g_0(z) \end{pmatrix}\left[A\overline{A} + B\overline{B}\right] \\ &+ \begin{pmatrix} f_3(z) \\ g_3(z) \end{pmatrix}\left[A\overline{B}e^{i\alpha(x(1-\cos\phi)+y\sin\phi)} + \text{c.c.}\right] \\ &+ \begin{pmatrix} f_4(z) \\ g_4(z) \end{pmatrix}\left[AB e^{i\alpha(x(1+\cos\phi)-y\sin\phi)} + \text{c.c.}\right]. \end{aligned} \tag{52}$$

The f_j and g_j functions satisfy the equations,

$$\begin{aligned} &f_2'' - 4\alpha^2 f_2 - Ra_0\, g_2' = 0, \\ &g_2'' + (Ra_0 - 4\alpha^2)g_2 - f_2' = Ra_0\, g_1 g_1' - f_1' g_1 + \alpha^2 f_1 g_1, \end{aligned} \tag{53}$$

$$\begin{aligned} &f_0'' - Ra_0\, g_0' = 0, \\ &g_0'' + Ra_0\, g_0 - f_0' = 2\left[Ra_0, g_1 g_1' - f_1' g_1 - \alpha^2 f_1 g_1\right], \end{aligned} \tag{54}$$

$$\begin{aligned} &f_3'' - \alpha^2(2 - 2\cos\phi) f_3 - Ra_0\, g_3' = 0, \\ &g_3'' + \left[Ra_0 - \alpha^2(2 - 2\cos\phi)\right] g_3 - f_3' = 2\left[Ra_0\, g_1 g_1' - f_1' g_1 - \alpha^2 f_1 g_1 \cos\phi\right], \end{aligned} \tag{55}$$

$$\begin{aligned} &f_4'' - \alpha^2(2 + 2\cos\phi) f_4 - Ra_0\, g_4' = 0, \\ &g_4'' + \left[Ra_0 - \alpha^2(2 + 2\cos\phi)\right] g_4 - f_4' = 2\left[Ra_0\, g_1 g_1' - f_1' g_1 + \alpha^2 f_1 g_1 \cos\phi\right], \end{aligned} \tag{56}$$

while the boundary conditions are,

$$
\begin{aligned}
z = 0: \quad & g_2' = [2\alpha d_1 \coth 2\alpha d_1]\, g_2, \\
& g_0' = 0, \\
& g_3' = \left[\sqrt{2-2\cos\phi}\,\alpha d_1 \coth(\sqrt{2-2\cos\phi}\,\alpha d_1)\right] g_3, \\
& g_4' = \left[\sqrt{2+2\cos\phi}\,\alpha d_1 \coth(\sqrt{2+2\cos\phi}\,\alpha d_1)\right] g_4, \qquad (57) \\
z = 1: \quad & g_2' = -[2\alpha d_3 \coth 2\alpha d_3]\, g_2, \\
& g_0' = 0, \\
& g_3' = -\left[\sqrt{2-2\cos\phi}\,\alpha d_3 \coth(\sqrt{2-2\cos\phi}\,\alpha d_3)\right] g_3, \\
& g_4' = -\left[\sqrt{2+2\cos\phi}\,\alpha d_3 \coth(\sqrt{2+2\cos\phi}\,\alpha d_3)\right] g_4, \qquad (58)
\end{aligned}
$$

while

$$
z = 0, 1: \quad f_j' = Ra_0\, g_j, \quad j = 0, 2, 3, 4. \qquad (59)
$$

References

Genç, G., Rees, D.A.S.: Onset of convection in horizontally partitioned porous layers. Phys. Fluids (2011)

Horton, C.W., Rogers, F.T.: Convection currents in a porous medium. J. Appl. Phys. **16**, 367–370 (1945)

Lapwood, E.R.: Convection of a fluid in a porous medium. Proc. Camb. Philos. Soc. **44**, 508–521 (1948)

Masuoka, T., Katsuhara, T., Nakazono, Y., Isozaki, S.: Onset of convection and flow patterns in a porous layer of two different media. Heat Transf. Japan. Res. **7**, 39–52 (1979)

McKibbin, R., O'Sullivan, M.J.: Onset of convection in a layered porous medium heated from below. J. Fluid Mech. **96**, 375–393 (1980)

McKibbin, R., O'Sullivan, M.J.: Heat transfer in a layered porous medium heated from below. J. Fluid Mech. **111**, 141–173 (1981)

McKibbin, R., Tyvand, P.A.: Thermal convection in a porous medium composed of alternating thick and thin layers. Int. J. Heat Mass Transf. **26**, 761–780 (1983)

Mojtabi, A., Rees, D.A.S.: The effect of conducting bounding plates on the onset of Horton-Rogers-Lapwood convection. Int. J. Heat Mass Transf. **54**(3), 293–301 (2011)

Newell, A.C., Whitehead, J.A.: Finite bandwidth, finite amplitude convection. J. Fluid Mech. **38**, 279–303 (1969)

Nguyen-Quang, T., Guichard, F., Nguyen, T.H.: Spatial pattern formation of motile microorganisms: from gravititactic bioconvection to protozoan culture dynamics. In: Vafai, K. (ed.) Porous Media: Applications Biological Systems and Technology, pp. 535–567. CRC Press, Boca Raton (2010)

Nield, D.A., Bejan, A.: Convection in Porous Media, 3rd edn. Springer, New York (2006)

Pop, I., Ingham, D.B.: Convective Heat Transfer: Mathematical and Computational Modeling of Viscous Fluids and Porous Media. Pergamon, Oxford (2001)

Postelnicu, A.P.: Thermal stability of two fluid porous layers separated by a thermal barrier. In: Proceedings of the 3rd Baltic Heat Transfer Conference, Gdansk, Poland, pp. 443–450 (1999)

Rana, R., Horne, R.N., Cheng, P.: Natural convection in a multi-layered geothermal reservoir. ASME J. Heat Transf. **101**, 411–416 (1979)

Rees, D.A.S.: The stability of Darcy–Bénard convection. In: Vafai, K. (ed.) Handbook of Porous Media, pp. 521–558. Marcel Dekker, New York (2000)

Rees, D.A.S.: Stability analysis of Darcy-Bénard convection. In: Lecture notes for the Summer School on Porous Medium Flows, Neptun, Constanţa, Romania, 25–29 June 2001

Rees, D.A.S., Genç, G.: The onset of convection in porous layers with multiple horizontal partitions. Int. J. Heat Mass Transf. (2011) (to appear)

Rees, D.A.S., Riley, D.S.: The effects of boundary imperfections on convection in a saturated porous layer: non-resonant wavelength excitation. Proc. R. Soc. Lond. A **421**, 303–339 (1989a)

Rees, D.A.S., Riley, D.S.: The effects of boundary imperfections on convection in a saturated porous layer: near-resonant wavelength excitation. J. Fluid Mech. **199**, 133–154 (1989b)
Rees, D.A.S., Riley, D.S.: The three-dimensional stability of finite-amplitude convection in a layered porous medium heated from below. J. Fluid Mech. **211**, 437–461 (1990)
Rees, D.A.S., Selim, A., Ennis-King, J.P.: The instability of unsteady boundary layers in porous media. In: Vadász, P. (ed.) Emerging Topics in Heat and Mass Transfer in Porous Media, pp. 85–110. Springer, New York (2008)
Riahi, N.: Nonlinear convection in a porous layer with finite conducting boundaries. J. Fluid Mech. **129**, 153–171 (1983)
Tyvand, P.A.: Onset of Rayleigh-Bénard convection in porous bodies. In: Ingham, D.B., Pop, I. (eds.) Transport Phenomena in Porous Media II, pp. 82–112. Elsevier, New York (2002)